1

Introduction to Lidar

Ulla Wandinger

Leibniz Institute for Tropospheric Research, Permoserstraße 15,
D-04318 Leipzig, Germany (ulla@tropos.de)

1.1 Lidar and the Atmosphere

Atmospheric research nowadays is hard to conceive without the use of remote-sensing techniques. Light detection and ranging (lidar) is, along with radiowave detection and ranging (radar), one of the backbones of the research field that deals with the profiling of the atmosphere. High spatial and temporal resolution of the measurements, the possibility of observing the atmosphere at ambient conditions, and the potential of covering the height range from the ground to more than 100 km altitude make up the attractiveness of lidar instruments. The variety of interaction processes of the emitted radiation with the atmospheric constituents that can be used in lidar allow the determination of the basic atmospheric variables of state, i.e., temperature, pressure, humidity, and wind, as well as the measurement of trace gases, aerosols, and clouds.

Lidar has largely contributed to our knowledge of the Earth's atmosphere during the past decades. It is particularly useful for the investigation of highly variable atmospheric parameters. Lidar has the potential for the observation of processes on scales that extend from a few cubic meters and a few seconds to global, multi-year coverage. Lidar has been used to investigate turbulent processes and the diurnal cycle of the planetary boundary layer, including the measurement of water-vapor and ozone fluxes. Meteorological phenomena such as frontal passages, hurricanes, and mountain lee waves were studied. Lidar helps monitor emission rates and concentration levels of trace gases. The stratospheric ozone depletion is documented globally with lidar. The role of polar stratospheric clouds is investigated and the classification of

polar stratospheric clouds is based on their scattering properties as seen with lidar. Lidar is used to distinguish water droplets from ice crystals in clouds. Lidar contributes to our knowledge of the climatic effects of aerosols. The stratospheric perturbation after major volcanic eruptions has been studied and the intercontinental transport of air pollution, desert dust, and forest-fire smoke has been detected. In the mesosphere, lidar has proven the existence of layers of metallic atoms and ions and of gravity waves therein. Lidar instruments can operate from the ground or from aircraft, one system has been flown on the Space Shuttle, and in the near future satellite-based lidar instruments will carry out global observations of atmospheric constituents from space. These and many more aspects of lidar are presented in this book giving an overview on the state of the art of the basic lidar techniques used in the investigation of the Earth's atmosphere.

1.2 Lidar History

The introduction of the lidar principle dates back to pre-laser times. In the 1930s first attempts were made to measure air density profiles in the upper atmosphere by determining the scattering intensity from searchlight beams [1–4]. Height information was obtained by scanning the receiver field of view of a distant telescope along the continuous light beam [5]. In 1938, pulses of light were used for the first time to measure cloud base heights [6]. The generation of light pulses by electric sparks and flashlamps allowed the replacement of the bistatic configuration by a monostatic setup, i.e., a setup in which transmitter and receiver are collocated and the height information is actively deduced from a measurement of the round-trip time between pulse emission and signal detection. The acronym lidar for this kind of measurement technique was first introduced by Middleton and Spilhaus in 1953 [7].

The rapid development of modern lidar technology started with the invention of the laser in 1960 [8] and the giant-pulse or Q-switched laser in 1962 [9]. Fiocco and Smullin published atmospheric observations with a ruby laser in 1963 [10]. About a decade later all basic lidar techniques had been suggested and demonstrated. Consequently, the first textbook on lidar edited by E.D. Hinkley [11] appeared in 1976. Ever since, success in lidar development was strongly connected with progress in optical and electronic technology, in particular

laser technology. Lidar researchers have always been involved in laser development. Many instruments use lasers specifically designed for lidar to meet the high requirements of certain lidar techniques on laser power, wavelengths, pulse width, beam shape, and spectral purity often not fulfilled by commercial products. In addition to lasers, optical filters with high transmissivity, narrow bandwidth, steep spectral slopes and/or high out-of-band suppression, efficient detectors for broad wavelength regions, data-acquisition systems with a dynamic range of several orders of magnitude, and computers that can process large amounts of data with high repetition rate belong to the devices needed for advanced lidar systems. Lidar has therefore always been both a source and a beneficiary of technological innovation.

1.3 Lidar Setup

The basic setup of a lidar system is shown in Fig. 1.1. In principle, a lidar consists of a transmitter and a receiver. Short light pulses with lengths of a few to several hundred nanoseconds and specific spectral properties are generated by the laser. Many systems apply a beam expander within the transmitter unit to reduce the divergence of the light beam before it is sent out into the atmosphere. At the receiver end, a telescope collects the photons backscattered from the atmosphere. It is usually followed by an optical analyzing system which, depending on the application, selects specific wavelengths or polarization states out of the collected light. The selected radiation is directed onto a detector,
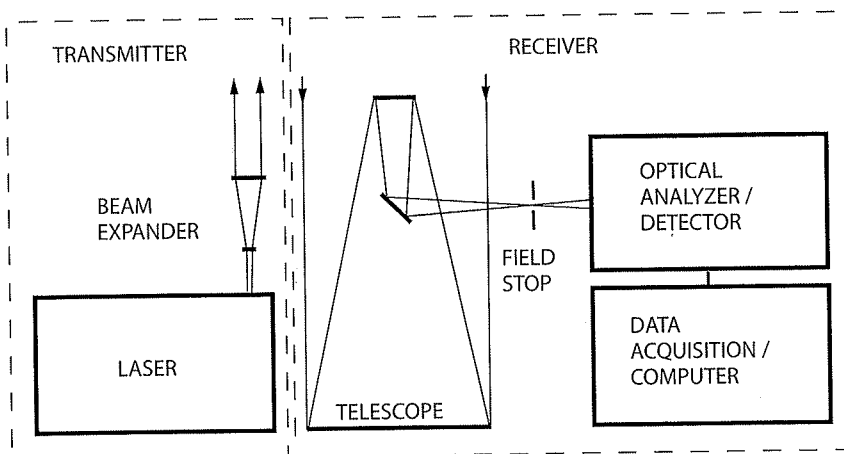

Fig. 1.1. Principle setup of a lidar system.

where the received optical signal is converted into an electrical signal. The intensity of this signal in its dependence on the time elapsed after the transmission of the laser pulse is determined electronically and stored in a computer.

Wavelengths used in lidar depend on the application and extend from about 250 nm to 11 μm. While ruby, nitrogen, copper-vapor, and CO_2 lasers were mainly used in the early years, high-power excimer and Nd:YAG lasers have been spreading out in the field since the 1980s. Excimer lasers produce ultraviolet radiation, whereas the Nd:YAG crystal emits in the infrared spectral region at a wavelength of 1064 nm. Frequency doubling and tripling with nonlinear crystals is widely used to convert the primary Nd:YAG radiation to 532 and 355 nm. Quadrupling to 266 nm is also utilized. Both laser types serve not only as direct lidar emitters, but also to pump secondary laser sources. The radiation can be shifted to longer wavelengths by stimulated Raman scattering in gases such as hydrogen and deuterium. This technique is preferably applied in the ultraviolet for ozone differential-absorption lidar and solar-blind Raman lidar. Dye lasers pumped either with excimer or Nd:YAG lasers have been used for a long time to produce the specific wavelengths needed for differential-absorption and resonance-fluorescence lidar. Nowadays, they are more and more being replaced by tunable, solid-state lasers based, e.g., on titanium:sapphire or alexandrite crystals and by optical parametric oscillators. The doping of crystalline lattices, e.g., yttrium aluminium garnet (YAG), yttrium lithium fluoride (YLF), lutetium aluminium garnet (LuAG), or of glasses with active ingredients such as Nd, Ho, Tm, Cr, Er, or Yb, creates a wide range of infrared wavelengths, some of which are particularly well suited for Doppler lidar. Presently, new laser types such as slab, microchip, waveguide, and solid-state Raman lasers are under investigation for their possible use in lidar.

Although laser beams are already highly collimated, their divergence is often further reduced by beam expansion to values of the order of 100 μrad. Then, the field of view of the receiver telescope can be chosen as low as a few hundred μrad. This has several benefits. First of all, background light from the atmosphere is efficiently reduced. Second, fewer photons that underwent multiple scattering in the atmosphere are detected. Finally, a small field of view is necessary for lidar methods based on signal detection with high spectral resolution because of the small acceptance angles of the wavelength-selective optical devices. Depending on the purpose of the lidar, the diameter

of the primary telescope optics ranges from 0.1 to a few meters. The majority of lidars use mirror telescopes. Lenses can only be used for small-aperture receivers. The field of view is determined by a field stop in the focal plane of the receiver optics. Lidar systems for investigations of the higher atmosphere utilize a chopper at this position. The chopper opens the field stop only when light from the region of interest arrives and thus blocks the strong backscatter signal from the lower atmosphere to avoid an overload of the detectors.

The geometric arrangement of the emitter and receiver optics determines the degree of signal compression at distances close to the lidar. At short distances the laser beam cannot completely be imaged onto the detector. Thus, only a part of the actual lidar return signal is measured. This part varies with distance and depends on laser beam diameter, shape, and divergence, the telescope's imaging properties (focal-length-to-diameter ratio), the receiver field of view, and the location of emitter and receiver optical axes relative to each other. In coaxial systems the laser beam is emitted along the optical axis of the receiver telescope. In biaxial systems the optical axes are spatially separated by at least one radius of the telescope mirror, and the laser beam enters the telescope field of view from the side. The function resulting from the combination of all geometric effects is called the laser-beam receiver-field-of-view overlap function. Its value is zero at the lidar and becomes unity when the laser beam is completely imaged onto the detector through the field stop. For large telescopes the overlap function can affect the lidar return signal up to distances of several kilometers.

Optical analysis of the backscattered light is usually done before the detection. In the simplest case, an interference filter is placed in front of the detector. The filter transmits light in a certain passband around the wavelength of interest and suppresses light outside the transmission band, e.g., background radiation. Other applications require more sophisticated solutions for the spectral analysis. Polarizers, grating spectrometers, interferometers, and atomic-vapor filters belong to the elements applied. Some examples are explained in more detail below.

Signal detection is realized with photomultiplier tubes (PMTs) or photodiodes. With PMTs and avalanche photodiodes (APDs) operated in the Geiger mode photons can be counted individually. The photon-counting technique is very sensitive and is used when the backscatter signal is weak, e.g., when it results from a weak scattering process or when the investigated region is far away from the instrument. The number

of photon counts per time interval after emission of the laser pulse is stored. The resolved time interval Δt corresponds to an atmospheric range bin $\Delta R = c\Delta t/2$ given by the speed of light c and the factor $1/2$ because the light has to travel forth and back. Storing signals with a time resolution of 100 ns thus results in an atmospheric range resolution of 15 m, provided the laser pulse is shorter than ΔR. For strong backscatter signals, analog recording is the method of choice, i.e., the average current produced by the photo pulses is measured, followed by analog-to-digital (AD) signal conversion and digital signal processing. In this case, the AD conversion rate determines the achievable range resolution of the system. Laser pulse repetition rates range from a few up to several thousand shots per second. Because the corresponding high time resolution is not meaningful, lidar signals are normally averaged over time intervals of a few seconds to minutes to reduce the amount of data that must be stored. A few applications require single-shot processing before averaging and need fast computer processing.

1.4 Lidar Equation

In the simplest from, the detected lidar signal can be written as

$$P(R) = KG(R)\beta(R)T(R), \qquad (1.1)$$

i.e., the power P received from a distance R is made up of four factors. The first factor, K, summarizes the performance of the lidar system, the second, $G(R)$, describes the range-dependent measurement geometry. These two factors are completely determined by the lidar setup and can thus be controlled by the experimentalist. The information on the atmosphere, and thus all the measurable quantities, are contained in the last two factors of Eq. (1.1). The term $\beta(R)$ is the backscatter coefficient at distance R. It stands for the ability of the atmosphere to scatter light back into the direction from which it comes. $T(R)$ is the transmission term and describes how much light gets lost on the way from the lidar to distance R and back. Both $\beta(R)$ and $T(R)$ are the subjects of investigation and in principle unknown to the experimentalist.

Going into more detail, we can write the system factor as

$$K = P_0 \frac{c\tau}{2} A\eta. \qquad (1.2)$$

P_0 is the average power of a single laser pulse, and τ is the temporal pulse length. Hence $E_0 = P_0\tau$ is the pulse energy, and $c\tau$ is the length of the volume illuminated by the laser pulse at a fixed time. The factor $1/2$ appears because of an apparent "folding" of the laser pulse through the backscatter process as illustrated in Fig. 1.2. When the lidar signal is detected at an instant time t after the leading edge of the pulse was emitted, backscattered light from the leading edge of the pulse comes from the distance $R_1 = ct/2$. At the same time, light produced by the trailing edge arrives from distance $R_2 = c(t - \tau)/2$. Thus $\Delta R = R_1 - R_2 = c\tau/2$ is the length of the volume from which backscattered light is received at an instant time and is called the "effective (spatial) pulse length." A is the area of the primary receiver optics responsible for the collection of backscattered light, and η is the overall system efficiency. It includes the optical efficiency of all elements the transmitted and received light has to pass and the detection efficiency. The telescope area A and the laser energy E_0, or, rather, the average laser power $\bar{P} = E_0 f_{\text{rep}}$, with the pulse repetition frequency f_{rep}, are primary design parameters of a lidar system. The experimentalist will also try to optimize the overall system efficiency η to obtain the best possible lidar signal.
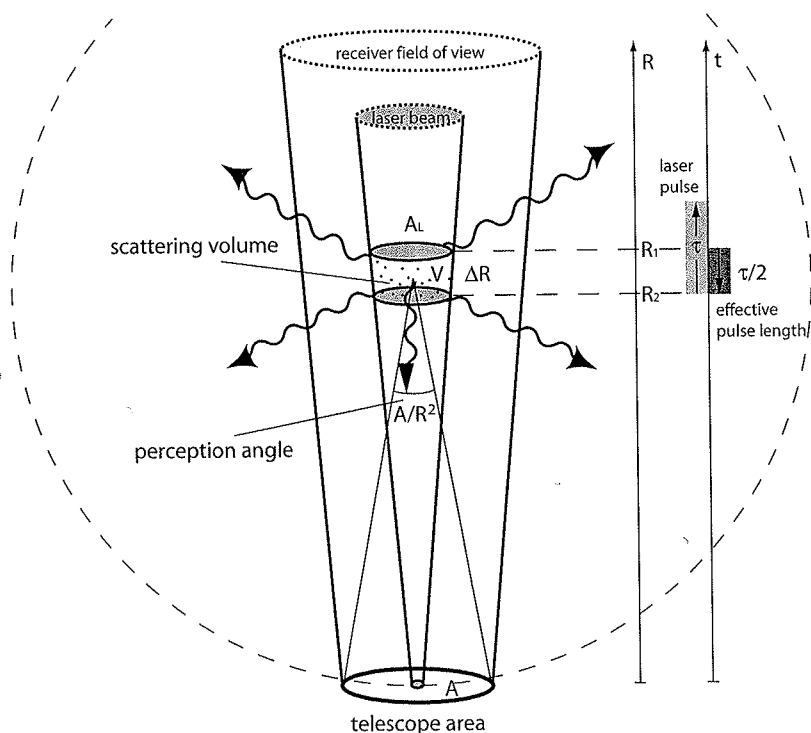

Fig. 1.2. Illustration of the lidar geometry.

The geometric factor

$$G(R) = \frac{O(R)}{R^2} \qquad (1.3)$$

includes the laser-beam receiver-field-of-view overlap function $O(R)$ described before and the term R^{-2}. The quadratic decrease of the signal intensity with distance is due to the fact that the receiver telescope area makes up a part of a sphere's surface with radius R that encloses the scattering volume (see Fig. 1.2). If we imagine an isotropic scatterer at distance R, the telescope area A will collect the fraction

$$\frac{I_c}{I_s} = \frac{A}{4\pi R^2} \qquad (1.4)$$

of the overall intensity I_s scattered into the solid angle 4π. In other words, the solid angle A/R^2 is the perception angle of the lidar for light scattered at distance R. The factor 4π does not appear explicitly in the lidar equation because it cancels out by the definition of the backscatter coefficient β as we will see below. It is primarily the R^{-2} dependence that is responsible for the large dynamic range of the lidar signal. If we start detecting a signal with $O(R) = 1$ at a distance of $10\,\mathrm{m}$, the signal will be 6 orders of magnitude lower at $10\,\mathrm{km}$ distance just because of the geometry effect. To what extent lidar is a *range-resolving and remote* measurement technique depends on our ability to compensate for this effect. Geometrical signal compression at short distances is one possibility as can be seen from Fig. 1.3 in which an arbitrary, but realistic overlap function is shown, multiplied with the function R^{-2}. The strong signal in the near field is suppressed by several orders of magnitude. On a few occasions the atmosphere will help in compressing the signal by an increase of the backscattering at larger distances as we will see below. In most cases, however, the atmosphere causes an additional decrease of the signal with range.

The backscatter coefficient $\beta(R, \lambda)$ is the primary atmospheric parameter that determines the strength of the lidar signal. It describes how much light is scattered into the backward direction, i.e., towards the lidar receiver. The backscatter coefficient is the specific value of the scattering coefficient for the scattering angle $\theta = 180°$. Let N_j be the concentration of scattering particles of kind j in the volume illuminated by the laser pulse, and $d\sigma_{j,\mathrm{sca}}(\pi, \lambda)/d\Omega$ the particles' differential scattering cross section for the backward direction at wavelength λ. The
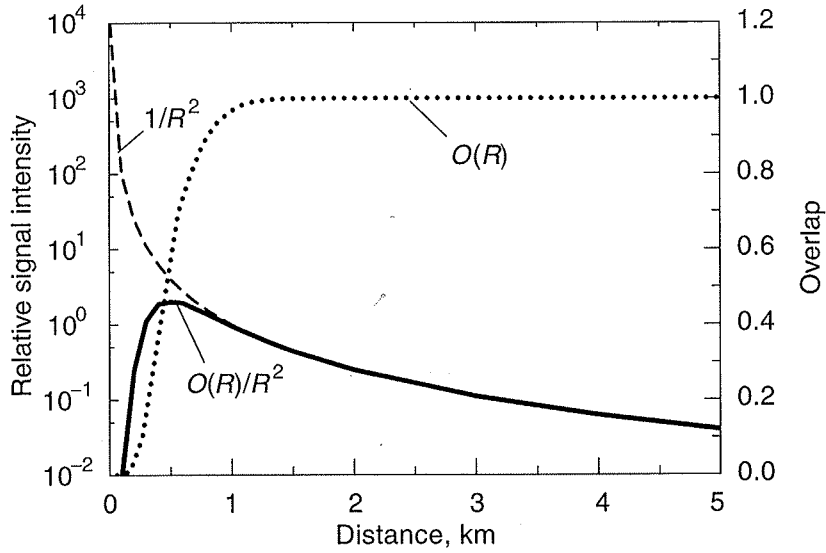
Fig. 1.3. Influence of the overlap function on the signal dynamics.

backscatter coefficient can then be written as

$$\beta(R, \lambda) = \sum_j N_j(R) \frac{d\sigma_{j,\mathrm{sca}}}{d\Omega}(\pi, \lambda), \tag{1.5}$$

with summing over all kinds of scatterers. Since the number concentration is given in units of m^{-3} and the differential scattering cross section in $m^2 sr^{-1}$, the backscatter coefficient has the unit $m^{-1} sr^{-1}$.

If we return to our simplified picture of isotropic scattering and assume that there is only one type of particle in the scattering volume, the relation between the backscatter coefficient and the isotropic scattering cross section σ_{sca} is $4\pi\beta = N\sigma_{\mathrm{sca}}$. The intensity of scattered light from the illuminated volume $V = A_L \Delta R = A_L c\tau/2$, with the laser-beam cross section A_L, is proportional to the area $A_s = N\sigma_{\mathrm{sca}} V$, i.e., the scattering cross section of all particles in the volume V. Thus, the relative intensity of the scattered light is

$$\frac{I_s}{I_0} = \frac{A_s}{A_L} = \frac{N\sigma_{\mathrm{sca}} c\tau}{2} = \frac{4\pi\beta c\tau}{2}. \tag{1.6}$$

With Eq. (1.4), we obtain the ratio of the collected to the emitted light intensity

$$\frac{I_c}{I_0} = \frac{A\beta c\tau}{2R^2}. \tag{1.7}$$

The right side of this equation describes that part of the lidar equation that directly refers to the scattering geometry, i.e., it contains the size and the backscatter properties of the scattering volume and the perception angle of the lidar.

In the atmosphere, the laser light is scattered by air molecules and particulate matter, i.e., $\beta(R, \lambda)$ can be written as

$$\beta(R, \lambda) = \beta_{\mathrm{mol}}(R, \lambda) + \beta_{\mathrm{aer}}(R, \lambda). \qquad (1.8)$$

Molecular scattering (index mol), mainly occurring from nitrogen and oxygen molecules, primarily depends on air density and thus decreases with height, i.e., backscattering decreases with distance if the observation is made from the ground, but increases in the case of downward-looking systems on aircraft or spacecraft. Particulate scattering (index aer for aerosol particles) is highly variable in the atmosphere on all spatial and temporal scales. Particles represent a great variety of scatterers: tiny liquid and solid air-pollution particles consisting of, e.g., sulfates, soot and organic compounds, larger mineral-dust and sea-salt particles, pollen and other biogenic material, as well as comparably large hydrometeors such as cloud and rain droplets, ice crystals, hail, and graupel.

As the final part of the lidar equation, we have to consider the fraction of light that gets lost on the way from the lidar to the scattering volume and back. The transmission term $T(R)$ can take values between 0 and 1 and is given by

$$T(R, \lambda) = \exp\left[-2 \int_0^R \alpha(r, \lambda)\, dr\right]. \qquad (1.9)$$

This term results from the specific form of the Lambert–Beer–Bouguer law for lidar. The integral considers the path from the lidar to distance R. The factor 2 stands for the two-way transmission path. The sum of all transmission losses is called light extinction, and $\alpha(R, \lambda)$ is the extinction coefficient. It is defined in a similar way as the backscatter coefficient as the product of number concentration and extinction cross section $\sigma_{j,\mathrm{ext}}$ for each type of scatterer j,

$$\alpha(R, \lambda) = \sum_j N_j(R)\sigma_{j,\mathrm{ext}}(\lambda). \qquad (1.10)$$

Extinction can occur because of scattering and absorption of light by molecules and particles. The extinction coefficient therefore can be

written as the sum of four components,

$$\alpha(R, \lambda) = \alpha_{\mathrm{mol,sca}}(R, \lambda) + \alpha_{\mathrm{mol,abs}}(R, \lambda) + \alpha_{\mathrm{aer,sca}}(R, \lambda)$$
$$+ \alpha_{\mathrm{aer,abs}}(R, \lambda), \qquad (1.11)$$

where the indices sca and abs stand for scattering and absorption, respectively. Because scattering into all directions contributes to light extinction, the (integral) scattering cross section σ_{sca}, together with the absorption cross section σ_{abs}, both in m^2, make up the extinction cross section,

$$\sigma_{\mathrm{ext}}(\lambda) = \sigma_{\mathrm{sca}}(\lambda) + \sigma_{\mathrm{abs}}(\lambda). \qquad (1.12)$$

Consequently, the extinction coefficient has the unit m^{-1}.

As indicated in the equations above, both β and α depend on the wavelength of the laser light. This wavelength dependence is determined by the size, the refractive index, and the shape of the scattering particles. We will discuss the consequences in conjunction with the description of the basic lidar techniques below.

Summarizing the discussion of the individual terms, we can now write the lidar equation (1.1) in a more common form as

$$P(R, \lambda) = P_0 \frac{c\tau}{2} A\eta \frac{O(R)}{R^2} \beta(R, \lambda) \exp\left[-2 \int_0^R \alpha(r, \lambda) \, dr\right]. \qquad (1.13)$$

This equation will be used, in the one or other variation, in the following chapters as the starting point of the description of the individual lidar techniques. One should mention that the detected signal will always consist of a background contribution P_{bg} in addition to the lidar signal described above. At daytime, the background signal is dominated by direct or scattered sunlight, whereas at nighttime the moon and the stars as well as artificial light sources contribute to the background light. Detector noise is another source of undesired signal. The background must be subtracted before a lidar signal can be evaluated further. Usually, a number of data points from either the far end of the signal, where no backscattered photons are expected any more, or from the period preceding the laser pulse emission are used to calculate the mean background signal $\bar{P}_{\mathrm{bg}}$ and the corresponding error ΔP_{bg} needed to compute the error of any quantity derived from the detected signals.

1.5 Lidar Techniques and the Contents of This Book

The contents of the book are arranged along the five basic lidar techniques which make use of specific interaction processes of the emitted radiation with the atmospheric constituents and which are:

- elastic-backscatter lidar,
- differential-absorption lidar,
- Raman lidar,
- (resonance) fluorescence lidar,
- Doppler lidar.

Each of the following chapters is self-sufficient and can in principle be understood without knowing any other chapter. It is therefore left to the reader which chapters he or she is interested to study and in which order. Chapters 2 and 3 of the book deal with polarization and multiple scattering, effects that, to a greater or lesser extent, play a role in all variants of the lidar technique. Chapters 4 to 12 describe the basic concepts, technical implications, and results that can be obtained with the most common types of lidar, following the classification given above. Chapter 13 is devoted to airborne and spaceborne applications, and chapter 14 introduces two techniques that are not yet widely applied. These two final chapters can be seen as a kind of outlook and motivation for further research on lidar techniques.

Elastic-backscatter lidar is the classic form of lidar and has in principle been fully described in the previous sections. In its simplest form it applies one laser emitting a single wavelength and one detector measuring the radiation elastically backscattered from the atmospheric molecules and particles. By elastic scattering we understand a process in which the wavelength of the radiation remains unchanged. This type of lidar delivers information on the presence and location of aerosol and cloud layers and is often called a Rayleigh–Mie lidar. We should, however, be careful when using this term and clarify what exactly we mean by Rayleigh and Mie scattering.

Rayleigh scattering can be defined as the elastic scattering from particles that are very small compared to the wavelength of the scattered radiation. In the context of lidar, Rayleigh scattering is always used as a synonym for molecular scattering. Since nitrogen and oxygen make up about 99% of the Earth's molecular atmosphere, we normally consider these two gases as the source of Rayleigh-scattered radiation.

The Rayleigh scattering intensity is proportional to λ^{-4} and dominates elastic-backscatter signals at short laser wavelengths. Somewhat different definitions exist concerning the spectral width of Rayleigh scattering. Temperature, pressure, and collective motion of the molecules lead to spectral broadening of the scattered radiation. The resulting intensity distribution of the elastically scattered light is called the Cabannes line. It has a spectral width of a few GHz or about $0.1\,\mathrm{cm}^{-1}$. If the elastic-backscatter signal is detected with low spectral resolution, rotational Raman scattering with much higher shifts, of the order of $100\,\mathrm{cm}^{-1}$, also contributes to the measured intensity. The sum of the Cabannes line and the rotational Raman bands on either side of it is therefore often referred to as Rayleigh scattering. On the other hand, Raman scattering is understood as an inelastic scattering process which involves the change of the energetic state of the molecule. From the point of view of Raman scattering theory, Rayleigh scattering is defined as the elastic scattering of radiation without a change of the vibrational–rotational quantum state of the interacting molecules and thus excludes rotational Raman scattering. We did not rule out one of the definitions in this book. Because of historic reasons and personal taste the reader will be confronted with both definitions in the literature anyhow. We tried, however, to make clear what the actual definition of the term is in the individual chapters.

Also the term *Mie scattering* is often used in a misleading way in the literature. The scattering theory developed by Gustav Mie [12] gives the analytical solution for scattering of radiation of arbitrary wavelength by a sphere of arbitrary radius and arbitrary complex refractive index. Thus, Mie scattering theory is not limited to a certain size of the scatterers, it even includes the solution for Rayleigh scattering. The term, however, is often used to describe the scattering from particles with sizes comparable to the wavelength of the radiation, or larger. The wavelength dependence of the scattered intensity is a function of particle radius relative to the wavelength and of the particles' complex refractive index. Small (Rayleigh) scatterers show the λ^{-4} dependence mentioned above. Scattering from very large particles does not depend on wavelength. In the region where particle radius and wavelength are of similar magnitude, the wavelength dependence of the scattering intensity varies strongly. Wavelength-dependent detection of light scattering can therefore be used to obtain information on size and other parameters of atmospheric aerosol particles in the radius range from about 50 nm to a few micrometers. The application of this technique requires

the emission of several laser wavelengths and an independent determination of the backscatter and extinction coefficients. Chapter 4 gives an overview on lidar measurements of aerosol particles and the inversion of multiwavelength data into microphysical particle properties.

Particles in the atmosphere have many different shapes. Therefore, Mie scattering theory is often a very rough approximation only. As long as the particles are small compared to the wavelength, the actual shape does not play a major role for the scattering properties as theories for non-spherical scatterers show. If the particles are large and non-spherical, like ice crystals, fluffy soot agglomerates, mineral dust, or sea-salt particles, we cannot use Mie scattering theory any more, but have to apply more elaborate non-spherical scattering theories. The presence of large non-spherical particles in the atmosphere can easily be detected with lidar. Spherical scatterers do not change the polarization state of linearly polarized laser light if scattered at 180°, whereas non-spherical scatterers lead to a depolarization of backscattered radiation. Polarization-sensitive light detection is particularly useful in the investigation of cirrus clouds and dust layers. The background and major findings of the polarization lidar technique are described in Chapter 2.

So far we assumed that each detected photon results from a single scattering process in the atmosphere. However, if the particle concentration is high and especially if the particles are large, as is the case in clouds, a photon can be scattered more than once before it reaches the lidar receiver. Again, the size of the particles plays an important role. Large particles show a strong forward-scattering peak due to light diffraction. Photons scattered at an angle close to 0° remain in the lidar's field of view, travel with the laser pulse, and can be backscattered (or the photon is backscattered and then undergoes one or several forward-scattering processes before reaching the detector). The effect of *multiple scattering* and how it can be corrected for or even exploited to provide information on cloud properties is described in Chapter 3.

Two special applications of elastic-backscatter lidar, the measurements of visibility and of cloud heights, are discussed in Chapter 6. These applications require comparably low instrumental effort and can routinely be used in traffic control, especially at airports.

A very specific form of an elastic-backscatter lidar is the high-spectral-resolution lidar described in Chapter 5. With an extremely narrow filter, realized by a Fabry–Perot etalon or an atomic-vapor or molecular-vapor absorption cell, the elastic backscatter signal from aerosol particles can be separated or removed from the molecular

backscatter component. The concept is based on the fact that, because of slow particle velocities, the spectral width of backscattering from particles is much narrower than the Cabannes line. Because the Rayleigh backscatter and extinction coefficients of the atmosphere can easily be calculated from pressure and temperature, the only unknown of a pure molecular backscatter signal is the particle extinction coefficient, which can thus be directly determined. The particle backscatter coefficient is independently inferred either from the signal transmitted by the Fabry–Perot etalon which contains virtually all of the aerosol, but only a small fraction of the molecular signal, or, in the case of the atomic or molecular cell filter, from the unfiltered signal. The same principle is used in the Raman lidar technique. Here, the molecular backscatter signal results from an inelastic Raman backscattering process from either nitrogen or oxygen as gases with known molecule number density in the atmosphere (see Chapter 4).

Raman scattering, as mentioned, is an inelastic scattering process which involves the change of the vibrational-rotational energy level of the molecule. The frequency shift of the scattered radiation corresponds to the energy difference between the initial and final molecular states and is thus specific for the interacting molecule. The change of rotational energy states leads to the rotational Raman side bands mentioned before. Because the population of energy levels follows Boltzmann's distribution law, the intensity distribution within the Raman bands contains information on the temperature in the scattering volume. One application of **Raman lidar** is therefore the measurement of atmospheric temperature profiles. This technique is described in Chapter 10. The change of the vibrational energy level results in frequency shifts of a few hundred to several thousand wavenumbers depending on the Raman-active molecule. Spectrally resolved analysis of backscattered radiation allows in principle the detection of a variety of atmospheric species. However, the comparably low Raman cross sections limit a meaningful use to gases present in relatively high concentrations. The Raman lidar technique is widely applied to the measurement of water vapor. The basic principles of Raman lidar, with special emphasis put on the observation of tropospheric water-vapor profiles, are explained in Chapter 9.

The detection of atmospheric gases with high sensitivity is possible with **differential-absorption lidar** or **DIAL**. The DIAL technique makes use of single absorption lines or broad absorption bands of gases. By emitting two wavelengths, one of which is absorbed more strongly than the other, the differential molecular absorption coefficient $\Delta\alpha_{mol,abs}$

is determined. If the differential absorption cross section $\Delta\sigma_{mol,abs}$ for the two wavelengths is known, the number concentration of the gas atoms or molecules can directly be deduced [see Eqs. (1.10)–(1.12)]. Chapter 7 introduces the application of DIAL for the measurement of gases such as O_3, NO_2, NO, N_2O, SO_2, CH_4, HCl, NH_4, and others. DIAL is also of great interest for the observation of water vapor as the most important atmospheric greenhouse gas. Because of the narrow absorption lines of the H_2O molecule, water-vapor DIAL requires high stability and spectral purity of the emitted laser light and the consideration of Doppler broadening of the backscattered light. Thus, Chapter 8 deals especially with water-vapor DIAL. In addition, this chapter discusses the potential of DIAL for temperature profiling. The latter technique uses the temperature-dependent strength of absorption lines of oxygen; in this case the number concentration of the gas is known and the differential absorption cross section is measured which contains the temperature information sought.

If the two DIAL wavelengths are spectrally separated by more than just a few nanometers as in the case of ozone DIAL, differential back-scattering due to the wavelength dependence of particle scattering becomes a major error source of this technique. The effect is hard to correct for if the particle scattering properties are not sufficiently well known. An alternative is the so-called **Raman DIAL**. Here, two nitrogen and/or oxygen Raman backscatter signals within the ozone absorption band are used to determine the ozone differential absorption coefficient. The differential backscatter coefficient is known in this case. The method is described as an application of Raman lidar in Chapter 9.

Two special forms of DIAL that may appear rather exotic even to long-term lidar practitioners are introduced in the final Chapter 14 of this book. BELINDA (for broadband-emission lidar with narrow-band determination of absorption), or "DIAL the other way around" as it is called by the authors, is based on the emission of laser radiation with a broader spectral width than the absorption line. The two DIAL signals are obtained by narrow-band filtering out portions of the backscattered light in the center and in the wings of the absorption line. With this approach the influence of line-broadening effects can be reduced. The price to pay is a large fraction of the backscatter signal lost in the filtering process. The second part of Chapter 14 describes white-light femtosecond lidar, a new and challenging approach of lidar. If the energy of a laser pulse is confined to a very short time interval of the order of femtoseconds, the pulse power can become as high as a few terawatts. At such high power,

qualitatively new interactions of the laser light with the surrounding medium occur. The non-linear Kerr effect leads to self-focusing of the laser beam in air, followed by plasma generation which in turn defocuses the beam and generates white light along the beam path. It was found that this white light predominantly travels in the backward direction, which makes it an excellent source for the use in lidar. On the way toward the receiver, the white light interacts with all atmospheric absorbers. Spectral analysis in the lidar receiver thus makes it possible to identify and quantify a multitude of atmospheric constituents. Even if a variety of technological and theoretical aspects have still to be solved and this technique cannot be applied to atmospheric research yet, it may give an idea of what kind the challenges of lidar research in the future may be.

Chapter 11 is the only chapter of this book that explicitly deals with the upper atmosphere. In the mesopause region, between about 80 and 110 km height, the presence of layers that contain metallic atoms and ions such as Na, K, Ca, Ca^+, Li, and Fe opened the field for **resonance fluorescence lidar**. Resonance fluorescence is obtained if the energy of the incoming photon coincides with the energy of a transition in an atom, ion, or molecule from one into another level. We speak of fluorescence because the reemission of light can occur at longer wavelengths. However, in this specific application the reemission is generally at the laser wavelength; therefore the technique is also called **resonance scattering lidar**. The extremely high cross sections for resonance scattering result in strong lidar signals and allow the determination of atom or ion number concentrations of less than 10^8 m^{-3} from distances of more than 100 km. In addition, the Doppler broadening and shift of the Na D_2 line can be used to determine temperature and wind in this remote region of the atmosphere.

Turbulence and wind are the macroscopic manifestation of the collective motion of atmospheric molecules and particles. Its component along the line of sight of the laser beam Doppler-shifts the backscattered radiation to higher frequency if the scatterers move toward the lidar, and vice versa. By determining the frequency shift the wind speed along the lidar line of sight can be measured. The frequency shift is proportional to the ratio of wind speed and the speed of light and is thus extremely small. The detection of such small frequency shifts requires special instrumental efforts. **Coherent Doppler lidar** is based on the emission of single-mode single-frequency laser radiation and the coherent detection of the radiation backscattered from the moving particles. The return signal is mixed with the radiation from a local oscillator, and the frequency difference is

determined. In order to also determine the sign of the shift and not just its magnitude, heterodyne detection is applied, i.e., a frequency offset is introduced between the emitted laser pulse and the local oscillator. **Direct-detection Doppler lidar** uses the molecular backscatter component and measures the frequency shift by applying narrow-band spectral filters. Chapter 12 explains the Doppler lidar technique.

The application of lidar not just from ground, but from airborne and even space-borne platforms is of special interest for regional and global monitoring of atmospheric constituents. To reliably run active remote sensors on flying platforms is a great challenge. The effort, however, is rewarded by an incredible new insight into atmospheric processes, as only active remote sensing has the potential for high-resolution observations in space and time. The LITE (Lidar In-space Technology Experiment) mission on board the Space Shuttle in 1994 has proven the viability of lidar for this type of application and certainly was one of the milestones in lidar history. Chapter 13 reports on this interesting aspect of lidar research and discusses the prospects.

References

[1] E.H. Synge: Phil. Mag. **9**, 1014 (1930)
[2] M.A. Tuve, E.A. Johnson, O.R. Wulf: Terr. Mag. **40**, 452 (1935)
[3] E.O. Hulbert: J. Optical Soc. Amer. **27**, 377 (1937)
[4] E.A. Johnson, R.C. Meyer, R.E. Hopkins, et al.: J. Optical Soc. Amer. **29**, 512 (1939)
[5] L. Elterman: J. Geophys. Res. **56**, 509 (1951)
[6] R. Bureau: La Météorologie **3**, 292 (1946)
[7] W.E.K. Middleton, A.F. Spilhaus: *Meteorological Instruments* (University of Toronto Press, Toronto 1953)
[8] T.H. Maiman: Nature **187**, 493 (1960)
[9] F.J. McClung, R.W. Hellarth: J. Appl. Phys. **33**, 828 (1962)
[10] G. Fiocco, L.O. Smullin: Nature **199**, 1275 (1963)
[11] E.D. Hinkley, ed., *Laser Monitoring of the Atmosphere* (Springer, Berlin 1976)
[12] G. Mie: Annalen der Physik, Vierte Folge **25**, 377 (1908)